A COMPARISON OF RESIDUAL STRESS IN HAMMER-PEENED, MULTI-PASS STEEL WELDS – A514 (S690Q) AND S41500


R. Simoneau


D. Thibault


J.-L. Fihey

ABSTRACT

As part of a program to assess the in-situ weldability and mechanical performance of the candidate high strength low alloy A514 (S690Q) steel as an alternative to the S41500 martensitic stainless steel for hydro-turbines, three aspects of the welds were studied: residual stress, Charpy toughness and cavitation erosion resistance. The experimental set-up involved robotized gas metal arc welding (GMAW), performed on U-groove and double-V weld preparation cut into 50 and 75 mm-thick steel plates. Half of the welds were robotically hammer-peened after each weld layer, except for the root pass. Strain gauges measured longitudinal and transverse strains during welding and hammer-peening. Once the weld cooled down to room temperature, the strain gauges provided the surface residual stress level at their location. Two-dimensional, sub-surface, longitudinal, residual stress distributions were measured on cut sections with the contour method, using an optical profilometer. The results showed that hammer-peening completely eliminates the near-surface tensile welding residual stress on the A514 steel, whereas on the S41500 steel, the process is less useful due to the already beneficial effect of the low temperature martensitic transformation during weld cooling. Furthermore, hammer-peening the last weld layer confines tensile residual stress inside the weld, while inducing compressive stress at the weld surface. Charpy test results showed that the A514 weld presented better toughness than the S41500 weld and comparable cavitation erosion resistance. Finally, hammer-peening showed a beneficial effect on cavitation resistance of the weld surface.

IIW-Thesaurus keywords: *Arc welding; Cavitation damage; Erosion; Gas shielded arc welding; GMA welding; Hardness tests; High strength steels; Martensitic stainless steels; Measuring instruments; Mechanical properties; Mechanical tests; Notch toughness; Reference lists; Residual stresses; Stainless steels; Steels; Strain gauges; Stress distribution; Toughness; Transformation; Turbines; Water turbines; Wear.*

Mr. Raynald SIMONEAU (simoneau.raynald@ireq.ca) and Mr. Denis THIBAULT (thibault.denis@ireq.ca) are Research Scientists at the Institut de Recherche d'Hydro-Québec, IREQ, Varennes, Québec (Canada). Mr. Jean-Luc FIHEY (jean-luc.fihey@etsmtl.ca), Director, is with the Department of Mechanical Engineering, École de Technologie Supérieure, Université du Québec, Montréal, Québec (Canada).

Doc. IIW-1942-08 (ex-doc. IX-2277r1-08/IX-L-1020r1-08) recommended for publication by Commission IX "Behaviour of metals subjected to welding".

INTRODUCTION

To optimize the construction and maintenance of its generating stations, Hydro-Québec, a mainly hydro-based generating utility (94 %), providing 180 TWh of energy and 35 500 MW of capacity to the province of Québec in Canada, is continuously developing and evaluating improved materials and processes. Examples of such developments via its Research Institute are a cavitation resistant stainless steel, now commercialized under the brand name CAVITEC®, and the portable six-axis SCOMPI® robot, which is widely used within

the company for *in situ* welding, precision grinding and hammer-peening interventions in the construction and maintenance of hydraulic generating stations such as penstock construction [1], gate and hydraulic runner refurbishment.

The Institute is currently in the process of assessing the *in situ* weldability and mechanical performance of the candidate high strength low alloy A514 (S690 Q) steel, as an alternative to the S41500 or CA6NM martensitic stainless steel for hydro-turbines [2]. When welding thick plates of these steels, hydrogen cracking is a concern. Thus, hydrogen input into the weld and residual stresses must be minimized. Other concerns are HAZ softening, toughness reduction and fatigue resistance. Controlled hammer-peening has the potential for both reducing the risk of hydrogen cracking and producing a more favourable distribution of residual stresses, in order to improve the fatigue resistance of the welds. Care must be taken, however, to avoid the risk of toughness degradation due to strain ageing [3].

EXPERIMENTAL APPROACH

Table 1 shows a summary of all experiments, test plate identification and results presented in the paper.

Materials, welding parameters and welding set-up

The weld tests were conducted on 50 mm (2 in-"2po") and 75 mm (3 in-"3po") thick quenched and tempered A514 (an equivalent of S690Q) high strength, low alloy steel plates and on 75 mm martensitic stainless steel S41500 (13Cr-4Ni). Two weld configurations were used: one-sided, 30 mm-deep, 45° U-groove and two-sided, 45°, half V-groove, full penetration butt joint for the 50 mm (2 in) A514 steel. The 300 mm-long test plates were instrumented with two strain gauges, positioned so as to monitor the evolution of thermal stresses during and after welding. Figure 1 shows the configuration of the test plates, the location of the strain gauges and thermocouples and shows the sequence of the weld beads. A robotized flux core welding process (FCAW) was used with the high strength low hydrogen flux-cored 1.2 mm wire, AWS A5.29 Class E110T5-K4 for the A514 steel, with the shielding gas 75 CO_2/25 % Ar.

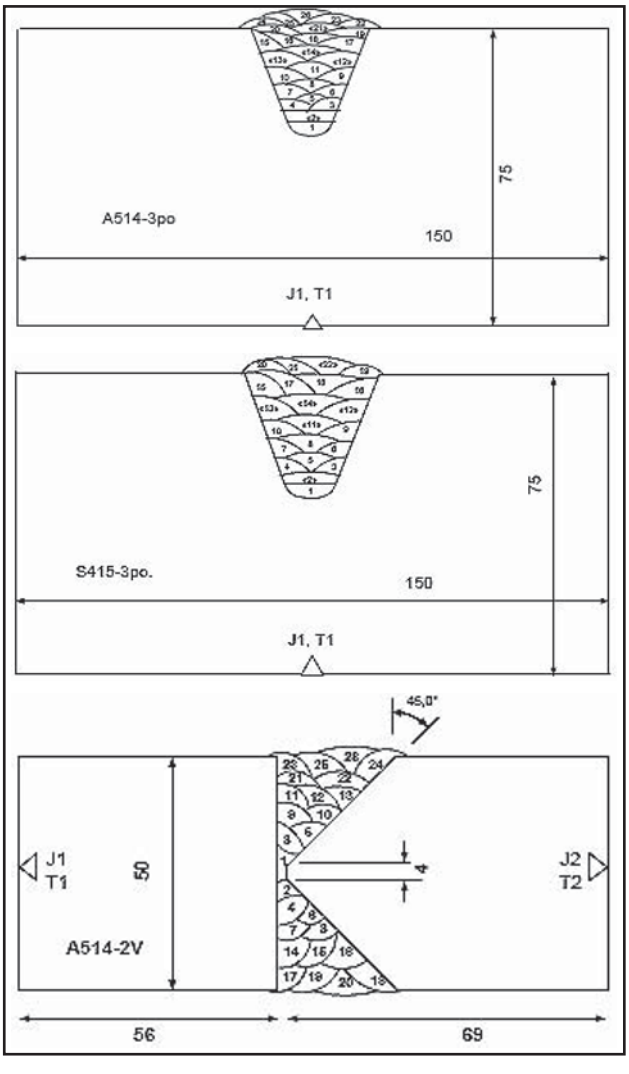

Figure 1 – Dimensions of the 3 weld test blocks with the location of the weld beads and of the strain gauges J1 and thermocouples T1

Table 1 – Summary of experiments and results presented

Identification	Plate thickness (mm)	Welding filler metal	Hammer-peening	Strain gauges	Contour method	Micro hardness	Charpy	Cavitation erosion
A514-2po-1	50	E110				√	√	
A514-2po-2	50	E110	√			√	√	
A514-3po-1	75	E110		√	√			√
A514-3po-2	75	E110	√	√	√			√
S415-3po-1	75	E410NiMo		√	√	√		√
S415-3po-2	75	E410NiMo	√	√	√	√		√
A514-2V-1	50	E110		√	√			
A514-2V-2	50	E110	√	√	√			
CA6NM	25						√	√
E410NiMo	25						√	√
Other turbine steels	25							√

Table 2 – Chemical analysis of the steel plates and welding wires (wt %)

	C	Si	Mn	P	S	Cr	Ni	Mo	V	Ti	Cu	Al	Nb	B	N
A514 2 po	0.16	0.25	1.41	0.011	0.001	0.23	0.07	0.495	0.019	0.004	0.01	0.06	0.016	0.002	0.003
A514 3 po	0.17	0.25	1.38	0.008	0.001	0.23	0.06	0.48	0.02	0.003	0.02	0.06	0.014	0.001	0.004
E110 Wire*	0.05	0.42	1.66	0.012	0.013	0.24	2.00	0.46							
S415 3po	0.01	0.46	0.84	0.021	0.004	12.2	4.6	0.61							
E410 NiMo*	0.023	0.35	0.53	0.01	0.006	12.8	4.0	0.47	0.002	0.001	0.06	0.02	0.005		0.06
*typical undiluted.															

For the S41500 steel a 1.2 mm metal core, AWS A5.29, type MC410NiMo, was used with the shielding gas 92 % Ar/8 % CO_2. Table 2 presents the chemical composition of the steel plates and of the welding wires. The mechanical properties are listed in Table 3. The preheat and maximum interpass temperature are presented in Table 4 with the welding parameters.

The one-sided weld test blocks were tack-welded to a rigid tubular steel fixture. The two-sided blocks were mechanically attached to the heated tubular fixture, in order to allow welding on both sides by reversing the blocks. Preheat was provided by two electric heaters located inside the tubular fixture situated under the plate. This temperature was maintained continuously from the beginning of the weld assembly until 16 hours after the end of welding, in order to avoid any hydrogen cracking risk.

Hammer-peening parameters

For the second test block for each of the three configurations, all of the weld beads were hammer-peened immediately after welding. A robot equipped with a force-controlled hammer was used. The same robot was used for peening and welding, thanks to an interchangeable, quick-connect tool adaptor. The hammer-peening parameters are presented in Table 5. A standard RRH06P Atlas Copco pneumatic hammer was used with a semi-spherical steel hammer head of 25 mm curvature radius and 15 mm shank diameter. This hammer struck blows of 6 J at a frequency of 36 Hz. The velocity and oscillation amplitude were adjusted to cover the full weld bead surface with a constant blow linear energy of 36 to 72 J/mm per pass. The robot maintained a controlled normal force of 105 N. The hammer-peening was executed at a temperature between 150 and 200 °C for the A514 steel and between 250 and 300 °C for the S415 steel during its martensitic transformation. On the A514 steel blocks, two peening passes were performed after each welding pass. On the S415 steel blocks, only one peening pass on each bead was made during the martensitic transformation, except for the last two weld layers, which were peened a second time between 150 and 200 °C. The peening temperature could be followed by a flying thermocouple (T4) thrown with a special spring-loaded device in the weld pool during welding.

Table 3 – Mechanical properties of the steel plates (measured) and welds (typical)

	Y.S. (MPa)	T.S. (MPa)	Elongation (%)
A514-2po	780	840	28
A514-3po	800	860	23
Weld E110*	720	820	20
S415-3po*	750	825	25
Weld E410*	750	900	16

Transient and residual stress measurement by strain gauges

Strain gauges were installed on each block to measure strain evolution during welding. The resistive gauges, type WK-06-125RA-350, were glued with a high temperature epoxy operating up to 250 °C. These were standard strain gauge rosettes that measure strain in three

Table 4 – Welding parameters

Bloc	No. layers/ beads	Speed (mm/s)	Oscill. (mm)	Current (A)	Voltage (V)	Welding linear energy (kJ/mm)	Dep. Rate (kg/h)	Preheat T. (°C)	Max. inter-p. T. (°C)
514-3po	9/27	6-6.7	0-2.2	290	33.3	1.4-1.6	6	100	160
415-3po	8/22	5.5-6.7	0-2.2	298	31.2	1.4-1.7	6	100	200
514-2V	11/26	6.7	0	281	33.8	1.4	6	100	160

Table 5 – Hammer-peening parameters

Steel	No. pass / bead	Energy per blow (J)	Impact freq. (Hz)	Head curv. radius (mm)	Speed (mm/s)	Osc. ampl. (mm)	Normal force (N)	Air press. (psi)	T (°C)
A514	2	6	36	25	3-6	1-7	105	90	150
S415	1	6	36	25	3-6	1-7	105	90	250-300

fixed directions, in order to allow the calculation of the principal stresses. On the one-sided weld blocks, the gauge J1 was located directly underneath the weld at mid-length of the plates. On the butt welded blocks, the gauges J1 and J2 were located on each side of the blocks at mid-thickness and mid-length as shown in Figure 1.

Residual stress measurement by the contour method

The longitudinal welding stress distribution was measured on cut cross-sections of the welded plates by the contour method developed by Prime [4-6]. All of the welded blocks were cut into two parts at half-weld length by electro-erosion with a 0.25 mm wire EDM (electrical discharge machine). The plate was held in a solid steel fixture during the cutting process in order to prevent any displacement of the block during the procedure [7]. The contour or shape of the two newly-created surfaces was measured with a 3-D chromatic aberration optical profilometer. The optical lens used had a 1.2 mm measuring range, a lateral x-y resolution of 2 μm and a vertical z resolution of 0.04 μm. The whole cut surface was scanned with measuring steps of 0.3 mm in the y direction (thickness) and 0.15 mm in the x direction (width). The two measured profiles were filtered, levelled with the mean value set at zero and added. Figure 2 shows an example of the result obtained on the A-514-3po block. After the addition of the two profiles, the values were inverted in order to have the area in tension marked positive and coloured red. The maximum deformation at the centre of the weld amounted to about 100 μm (200/2) for this area, which should have been at the yield strength of the A514 steel, 800 MPa. In comparison with the corresponding macrograph below, the weld residual tensile stress pattern was shifted to one side, where the last 3 beads have been deposited, with the last one close to the centre of the weld.

Residual stresses have been calculated according to the elastic superposition principle, by forcing the average measured surface on a flat surface in the finite element Ansys model with a 1 mm grid. The measured displacements were applied to the model as boundary conditions in a normal direction only, the other direction being left unconstrained. Finite element results were post-processed to obtain stress along the surface where displacements were applied. The final result was a cross-section mapping of the residual stresses that originally existed normal to the plane of the cut.

Hardness, toughness and cavitation erosion resistance

Vickers hardness measurements with a load of 5 kg were made every 0.5 mm on cut cross-sections across the four welds, without any post-weld heat treatment 3 mm under the weld surface.

The Charpy V-notch toughness of the A514-2po 50 mm plates has been measured at – 20 °C on 2 specimens, cut 1.5 mm below the surface of the U-shaped weld, according to ASTM standard A488-07, and 2 others on each plate at mid-thickness. The 10 mm notch length was cut normal to the surface through the thickness of the weld. Four specimens for each plate were also cut, with the notch located after etching in the inclined plane of the heat-affected zone (HAZ). For the S415 – E410NiMo steel, Charpy specimens with the same normal notch orientation were cut from different plates, welded with two different shielding gases, two different welding electrodes, one metal core and one flux core, as well as with and without stress relief heat treatment at three different temperatures, 580, 600 and 620 °C. For the purposes of comparison, toughness measure-

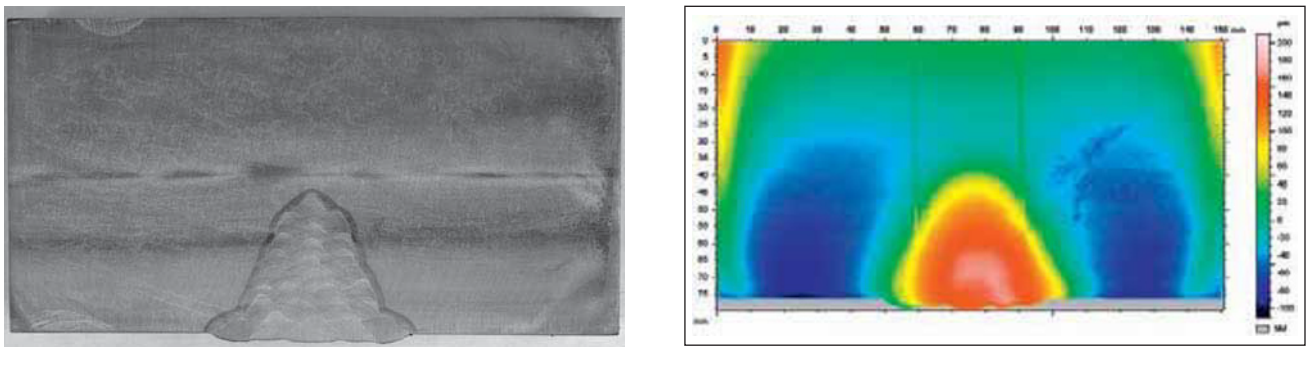

Figure 2 – Mean deformation (double-inverted) of the two transversal cut surfaces of the welded plate A514-3po, without peening, produced by the welding residual stress and corresponding macrograph

ments were also conducted at 0 °C on the S415 steel plate and on a sample of cast CA6NM turbine blade.

Cavitation erosion resistance of various hydro-turbine steels was measured in the high pressure cavitation jet apparatus of the Institute of Research of Hydro-Quebec (IREQ). This system produces large cavitation impacts similar to those encountered in large hydro-turbines [8-9]. In order to take into account the effect of the slight difference in nozzle geometry and water temperature on cavitation intensity, the weight loss erosion data were normalized to the weight loss of aluminium alloy 6061T6, measured between each test batch. The sapphire jet nozzle was 0.8 mm in diameter. The high pressure of the jet was set around 230 MPa, in order to obtain a weight loss rate of the aluminium alloy between 950 and 1 000 mg/h. The pressure of the tap water-filled jet chamber was maintained at 21 MPa over the ambient pressure. The temperature of the open circuit tap water was between 6 and 14 °C.

RESULTS

Welding transient stress

Figure 3 shows both principal stresses measured at the strain gauge J1 during welding and hammer-peening of bead 5 of the 3 in plates with a one-sided weld (A514 and S415). Figure 4 shows the maximum principal stresses of gauges J1 and J2 for the butt joint, double-V groove weld, on the 2 in plate during welding and hammer-peening of bead 5. Sp is the principal stress in the direction perpendicular to the weld length and sq, the principal stress in the direction parallel to the weld length. Sp1 and sq1 are calculated from gauge J1 measurements and sp2 and sq2 from gauge J2.

On the one-sided welds in Figure 3, at the start of welding, the transient heating due to welding produces transverse and longitudinal bending compression or a decrease of tensile stress (positive) at J1, located underneath the weld, 45 mm from the fusion line (see Figure 1). At about mid-length of the bead deposit, the weld cooling reverses the stress variation, decreasing compression or increasing tensile stress at the back centre of the plate. The tensile stress reaches its maximum at about 60 seconds after the weld start; in a longer time frame, the tensile stress relaxes on the A514, due to thermal diffusion and temperature homogenization throughout the plate thickness. For the S415 (c), this stress relaxation or decrease is more pronounced due to the lower temperature (200-300 °C) martensitic transformation and dilatation. The temperature variations are faster on the A514 than on the S415, due to the former's higher thermal conductivity.

A small effect of the higher temperature martensitic transformation of the A514 steel may be seen before the welding tensile stress reaches its maximum both on plate A514-3po, [Figure 3 a)], and on A514-2V

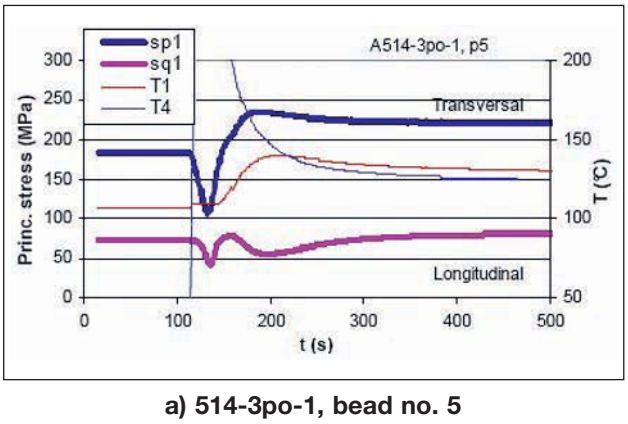

a) 514-3po-1, bead no. 5

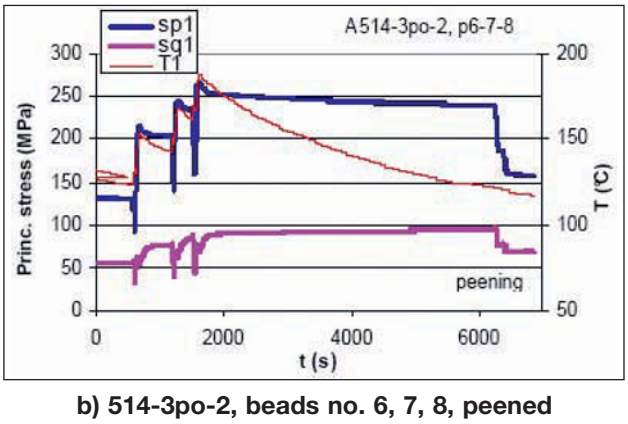

b) 514-3po-2, beads no. 6, 7, 8, peened

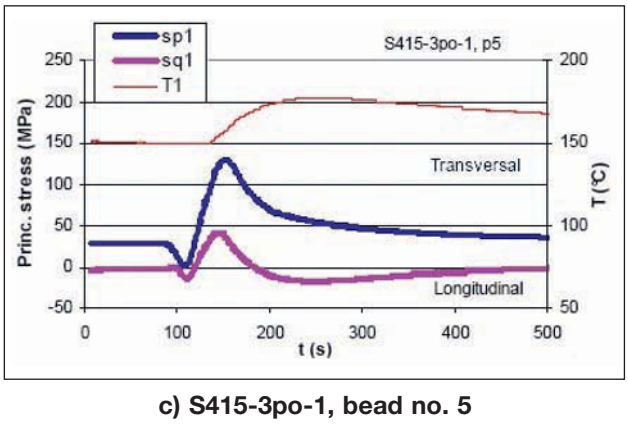

c) S415-3po-1, bead no. 5

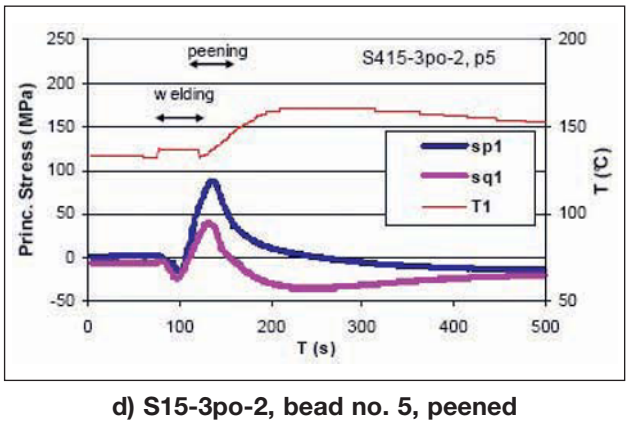

d) S15-3po-2, bead no. 5, peened

T1 is the temperature of the plate surface centre and T4 the temperature read by the flying thermocouple thrown in the weld pool.

Figure 3 – Principal stresses (sp1, sq1) measured at J1 during welding and peening individual beads on one-sided plates

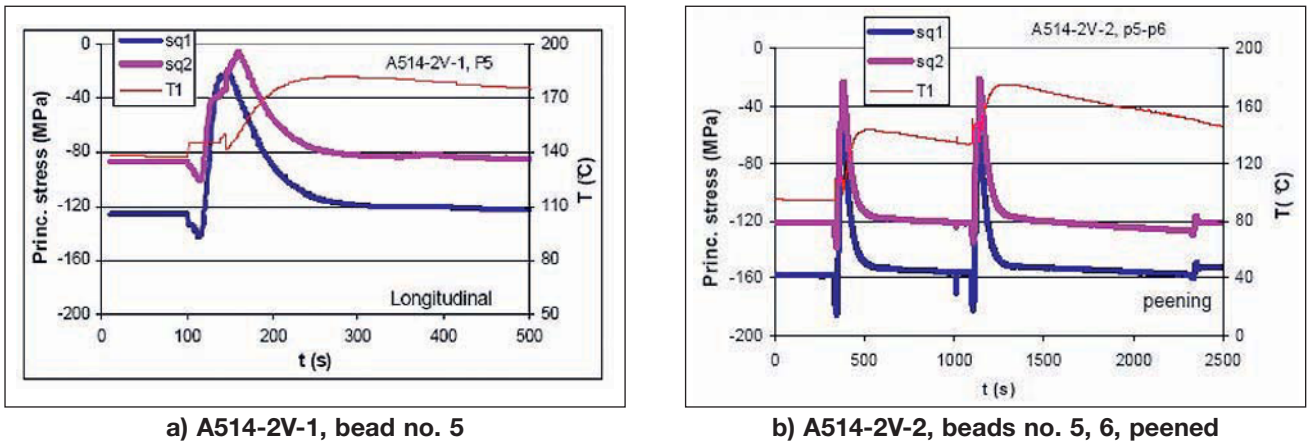

a) A514-2V-1, bead no. 5 **b) A514-2V-2, beads no. 5, 6, peened**

Figure 4 – Maximum principal stress measured by J1 (sq1) and J2 (sq2) on the double-sided V-joint in A514 steel

[Figure 4 a°)], with a slowing down of the tensile stress accumulation and a break in slope before it reaches its maximum.

On the butt joint configuration, A514-2V (Figure 4), the weld heating reduces the compressive longitudinal stresses measured by J1 and J2 on the plate sides, while the subsequent weld cooling reinstalls them. Hammer peening is seen to effectively reduce the transverse tensile stress of the one-sided weld [Figure 3 b)]. The effect is much less consequential on the longitudinal compressive stress of the double-V weld.

Residual stress measured by the strain gauges

Figure 5 and Figure 6 present the principal residual welding stress, the transverse stress, as measured by strain gauge J1 at the back of the four one-sided welded plates. Two assumptions can therefore be made: that the material is behaving elastically and that initially, the plate did not contain any residual stress.

On the thicker, 75 mm, A514 plate, the weld produces transversal stress reaching 500 MPa at the end of the weld, as seen in Figure 5. The double hammer-peening of each bead reduces the final stress down to 280 MPa, a reduction of 44 %. On this thick, high strength plate, hammer-peening has an impressive effect on the transversal residual stress, even on the last weld layer.

On the S415 75 mm plate, the cumulative effect of the low temperature martensitic transformation is obvious. The final transversal stress with the same weld reaches only 170 MPa. Hammer-peening of each bead once produces a slight effect on the transversal stress. With the supplementary peening of the last two weld layers, the final stress is reduced to 100 MPa, a reduction of 40 %.

For all of the one-sided weld blocks, the transverse stress is the largest principal stress at the location of gauge J1 at the back centre of the blocks. For both steels, the longitudinal stress is about 40 % of the transversal stress for the 75 mm plate, with and without hammer-peening.

For the two-sided weld configuration, the blocks A514-2V, the largest principal stress at the location of gauges J1 and J2 on the side of the blocks is the longitudinal stress. In this case, the transversal stress is very small, smaller than 25 MPa. The mean values of the longitudinal stress at J1 and J2 are presented on Figure 7 for both plates with and without hammer peening. On the plate without hammer peening the first bead was deposited in two parts due to a torch problem, thus producing a 50 MPa lower stress than the same bead on the plate with peening. This stress reduction stayed for the whole weld and would have produced a final residual stress 50 MPa lower at the end of the weld without peening. The final residual longitudinal stress without peening is -240 MPa; it could have been lower than -300 MPa without the first bead interruption. This is about 1/3 of the yield strength of this steel, which corresponds to the fact that the hea-

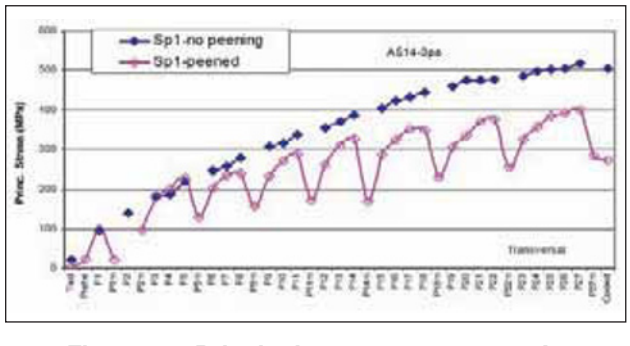

Figure 5 – Principal stresses at gauge J1 with and without peening during the welding of plate A514-3po

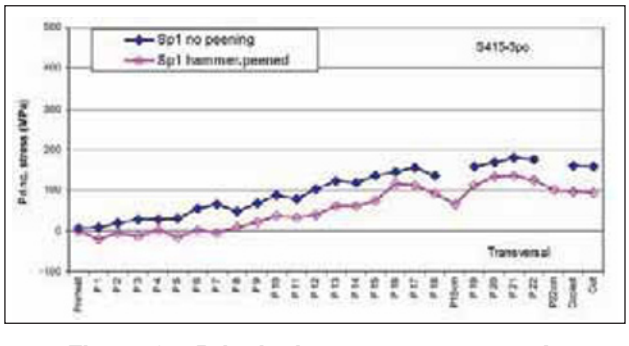

Figure 6 – Principal stresses at gauge J1 with and without peening during the welding of plate S415-3po

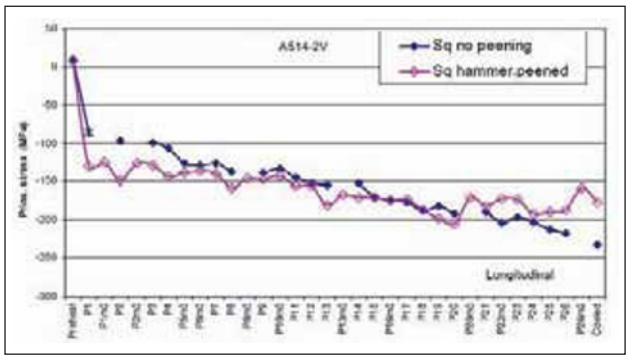

Figure 7 – Mean principal stress at gauge J1-J2 with and without peening during the welding of plate A514-2V

ted weld cross-section is about 1/3 of the plate cross-section, with the weld zone being stressed at the yield strength. The effect of hammer-peening on this longitudinal stress is quite slight for each peened bead and also for the total cumulative effect, with a final stress value of -175 MPa, a reduction of about 25 %. The lesser effect on longitudinal stress (25 %) than on transverse stress (44 %) can be explained by the location of the strain gauge on the back face: this location renders the gauge more "sensitive" to transverse stress applied at the surface, than to longitudinal stress applied at the surface, because of transverse plate bending.

Residual stress measured by the contour method

Figure 8 presents the residual stress measured by the contour method for the six welded plates without (left side) and with (right side) hammer-peening. The same stress scale is used for all the maps. The measurements have been extrapolated on each side of the weld to obtain a normal rectangle, in order to facilitate the finite element calculation. Figure 9 presents stress line profiles extracted from these contour method results for both 75 mm, one-sided welded plates. X profiles show the variation of the longitudinal residual stress along the X-direction, i.e. the length of the weld, for three Y positions close to the top of the plate, i.e. close to the weld surface. Y profiles show the variation of the same longitudinal residual stress through the thickness of the plate, perpendicular to the weld length, for two X positions close to the weld centre line.

The maximum, longitudinal, residual, tensile stress occurs in the E110 weld area about 10 mm under-

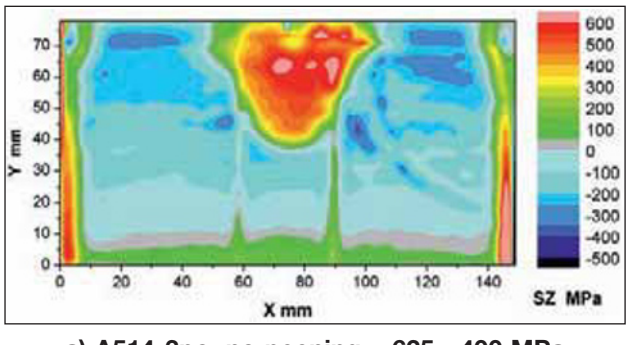

a) A514-3po, no peening, +625, -400 MPa

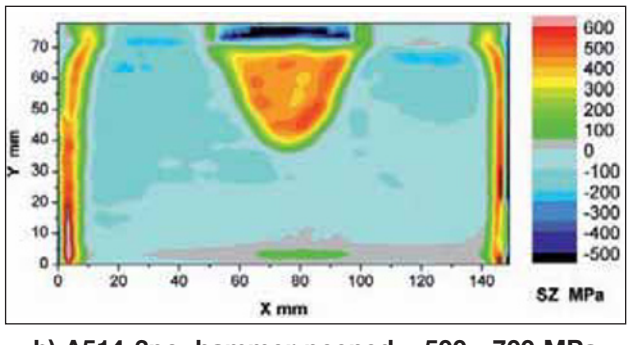

b) A514-3po, hammer-peened, +500, -700 MPa

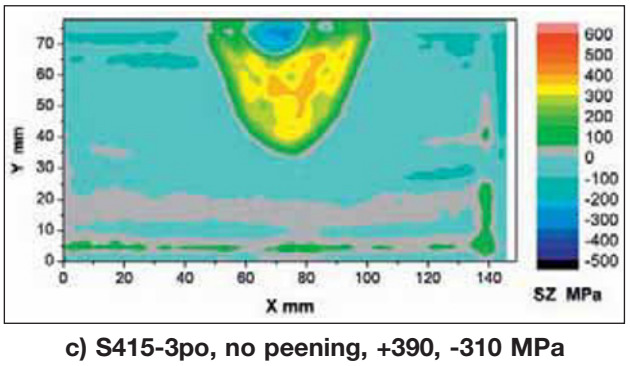

c) S415-3po, no peening, +390, -310 MPa

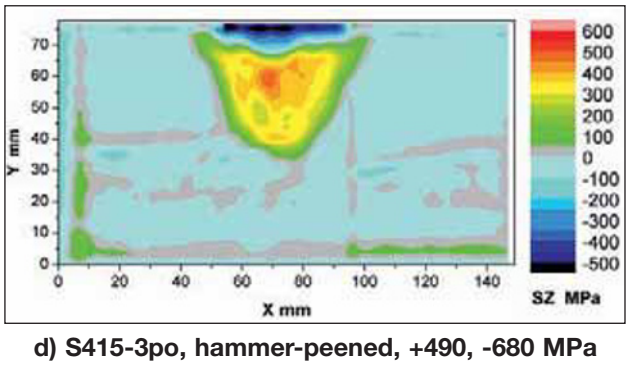

d) S415-3po, hammer-peened, +490, -680 MPa

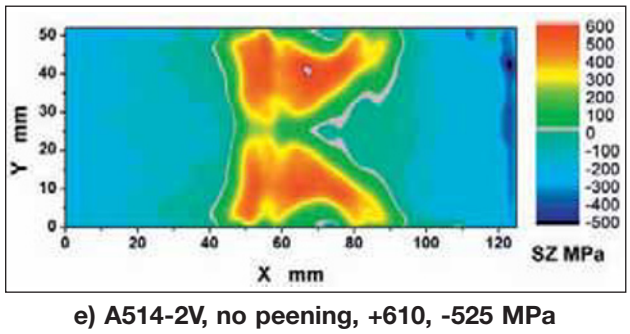

e) A514-2V, no peening, +610, -525 MPa

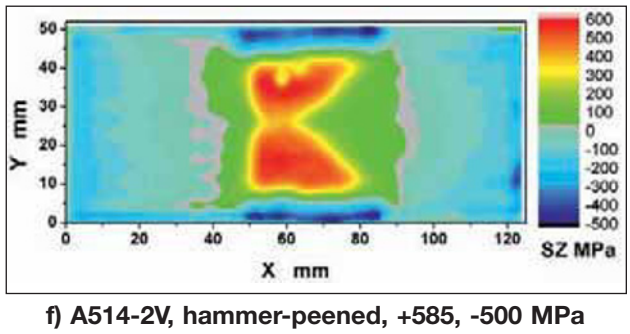

f) A514-2V, hammer-peened, +585, -500 MPa

Figure 8 – Longitudinal welding residual stress measured on all of the plate cross-sections by the contour method

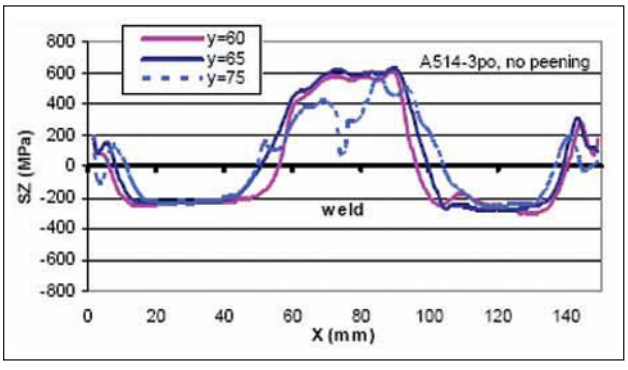

a) A514-3po, no peening, X profile

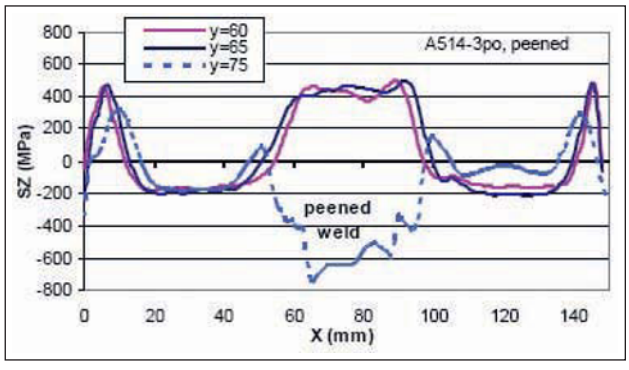

b) A514-3po, hammer-peened, X profile

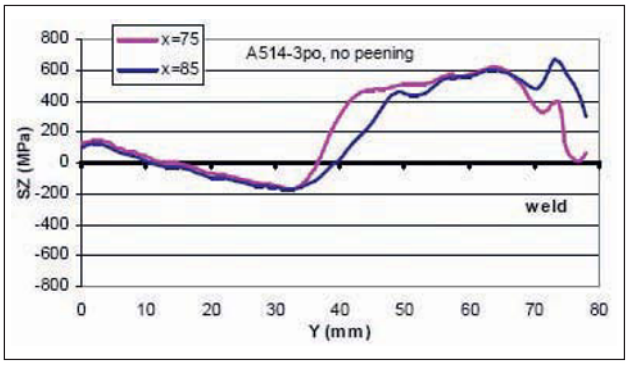

c) A514-3po, no peening, Y profile

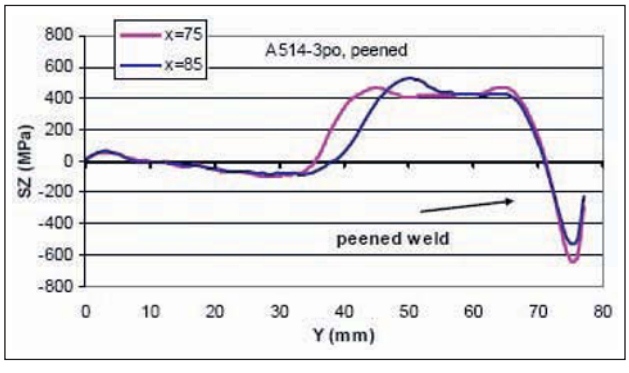

d) A514-3po, hammer-peened, Y profile

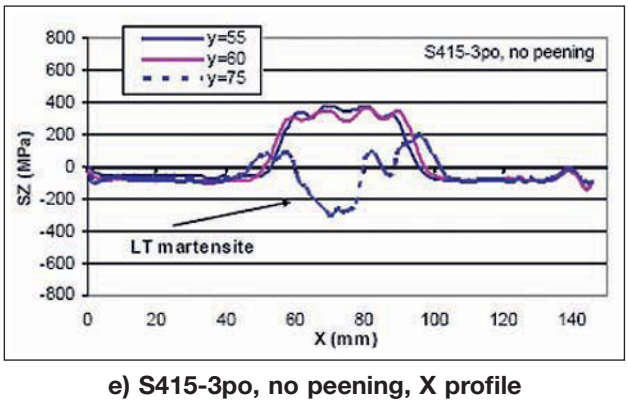

e) S415-3po, no peening, X profile

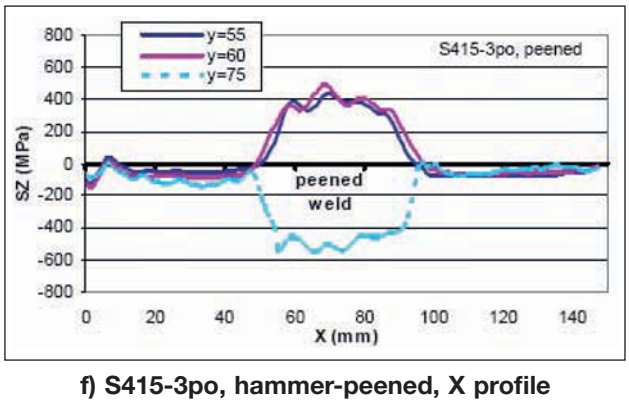

f) S415-3po, hammer-peened, X profile

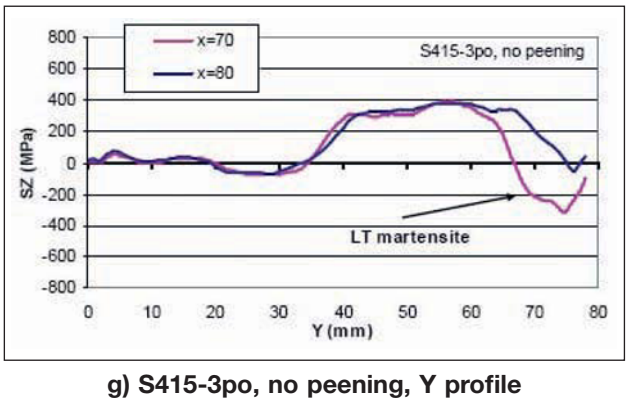

g) S415-3po, no peening, Y profile

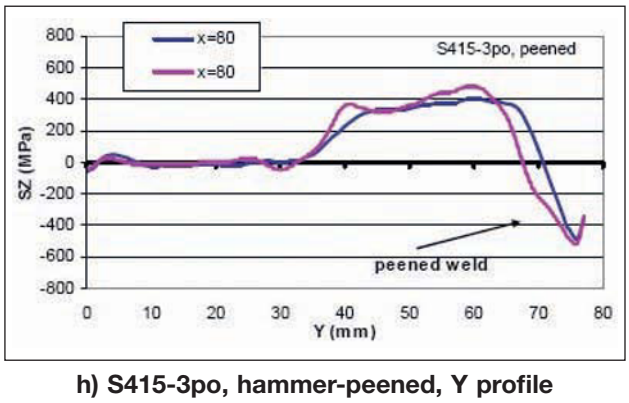

h) S415-3po, hammer-peened, Y profile

Figure 9 – Line profile of the longitudinal residual stress from the contour method for two steels

neath the surface in the A514-3po unpeened blocks. It is around 700 MPa for the 75 mm block, which is comparable to the 720 MPa yield strength of the E110 weld. Although the contour method is not as accurate for the first millimetre below the surface, due to the cutting and measuring processes, there is a clear decrease of the tensile stress from the centre to the surface of the weld, going from 700 down to about 300 MPa 1 mm from the surface. It is even lower at the location of the last central weld bead. This decrease is caused by faster cooling at the surface, the later cooling of the weld centre relaxing the surface tensile stress. It is also caused by the martensitic or bainitic transformation, especially for the last bead.

Hammer-peening decreases the average tensile stress of the weld to around 400 MPa and introduces a 6 mm high compression layer (500 to 700 MPa) at the weld surface. For the 75 mm blocks, the maximum compression of about 300 MPa is located midway between the weld and the side edges. On these blocks, the side surface on a 5 mm thickness show tensile stress, greater towards the back of the plate, probably caused by transverse bending due to the centre weld. For the same reason, there is some tensile stress at the back of the plate.

The great effectiveness of low temperature martensitic transformation is well-demonstrated on the stress mapping of the S415 blocks. The maximum tensile stress at the centre of the weld is only 390 MPa. A large portion of the cross-section has near-zero stress. There is almost no tensile stress at the surface of the weld. The last surface bead even shows compressive stress between 200 and 300 MPa. Hammer-peening has had little effect on the internal tensile stress. The last layer hammer-peening after the martensitic transformation has left a 6 mm compression zone.

For the full penetration two-sided weld on the 50 mm A514-2V plate, the maximum tensile stress of about 600 MPa is located at the centre of each one-sided weld. The whole central area is in tension with 500 MPa close to the surface. The largest compression, 400 MPa, is close to both side surfaces without hammer-peening. Hammer-peening on each side creates a 6 mm compression layer at the surface of the weld and confines tensile stress within the plate far from the surface.

The 6 mm compression layer produced by hammer-peening is clearly seen both on the mappings of Figure 8 for the three peened welds and on the Y profiles of Figure 9 for the two peened plates, where the residual stress is in compression from the peened surface (Y = 77 mm) down to 6 mm below the surface (Y = 71 mm).

Comparison of contour and strain gauge measurement of residual stress

Figure 10 compares the maximum, longitudinal, residual stress measured by the strain gauge, SLj, and by the contour method at the same location of J1, SLc j. It also compares for the three blocks, with and without peening, the maximum stress measured by the contour method inside the weld, SLc w, and at the weld surface, SLc ws. Although the residual longitudinal stresses are rather low at the gauge location, there is a fair agreement between both techniques. The beneficial effect of the low temperature martensitic transformation of the S415 steel on the maximum tensile stress within and at the surface of the weld, is well illustrated in that Figure. It is also the case of the high compressive stress produced by hammer-peening at the weld surface, as found in another study [10]. This behaviour of the martensitic stainless steel S415 is a precious advantage for controlling residual stress, cold cracking and distortion during fabrication of large hydro-turbines [11-12]. The low temperature martensite transformation of this steel should also improve the fatigue life of hydro-turbine runners [13-14].

Hardness and toughness

Figure 11 presents hardness measurements on cut cross-sections across the weld of both steel welds, without any post-weld heat treatment. On the E110 of the A514 block, the higher transformation temperature made possible the softening of the major part of the weld, except for each HAZ on each side, because of the greater hardenability of the plate steel. The slight hardening effect of the last hammer-peened layer can also be seen. The greater hardenability of the higher alloy S415 and E410NiMo produces an important hardening of the weld zone. The heat-treating effect of the subsequent neighbouring weld bead manages to soften only a thin layer of each bead, as revealed by the three hardness depressions in the weld zone E410NiMo of the S415 block.

The different hardening behaviour of these steels has an important effect on the as welded toughness as presented in Figure 12. The very clean A514 steel tested shows remarkable toughness at -2 °C of 260 J for the 50 mm plate and 160 J for the 75 mm plate. Good toughness is also measured in the E110 weld, having a very fine microstructure, even in the HAZ. Two different E410NiMo welding wires have been tested, one metal core wire, MC, with and without a thermal treatment of one hour at 620 °C (T3), one flux core wire, FC, with a thermal treatment of one hour at 600 °C (T1) and

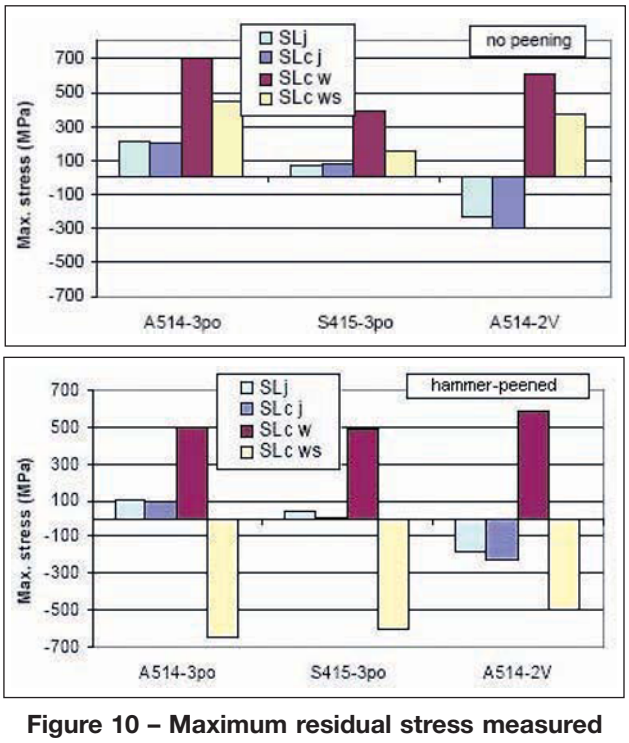

Figure 10 – Maximum residual stress measured at 4 locations on the 8 welded plates, with and without hammer-peening, with the strain gauge (SLj) and with the contour method, at 3 locations, at the strain gauge location (SLc j), within the weld (SLc w) and at the weld surface (SLc ws)

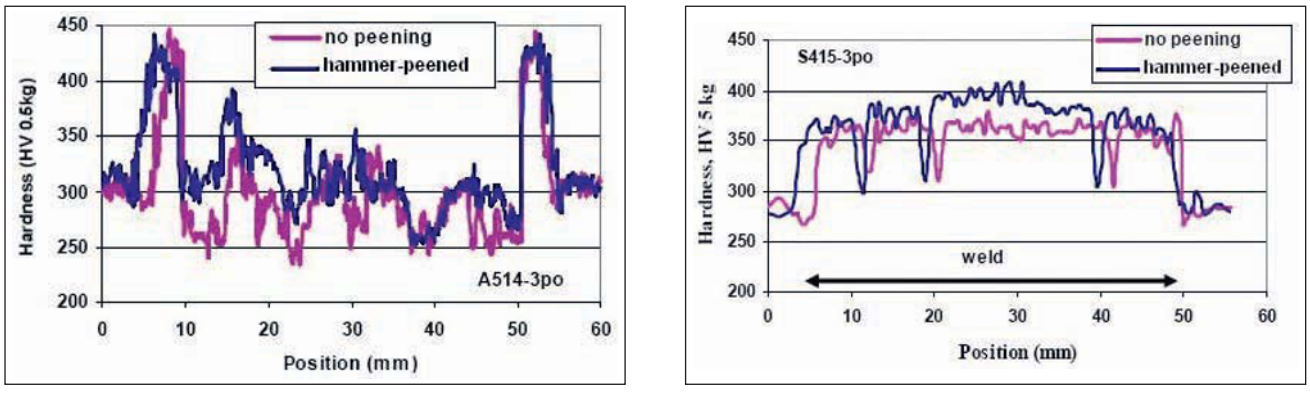

Figure 11 – Hardness profile measured across the weld, 2 mm below the surface of both steels

at 580 °C (T2). The non-heat-treated E410NiMo weld offers poor toughness, as low as 20 J at 0 °C. Even with the best welding practice and heat treatment, weld toughness is not higher than 50 J, whereas the low carbon S41500 material (rolled) shows 160 J and the cast CA6NM sample 70 J.

Cavitation erosion resistance

Figure 13 presents the cavitation erosion resistance of various hydro-turbine steels, as measured in the high pressure IREQ cavitation jet apparatus. The stainless steels used in turbines, S41500 equivalent to the cast CA6NM, the austenitic stainless steel S304L and their welding metals, E410NiMo and E308L, all have similar cavitation resistance, between ten and twelve times that of the aluminium 6061T6. Their resistance is twice that of plain carbon steel A516, equivalent to the cast A27 previously used in hydro-turbines. The high resistance martensitic carbon steel A514 and its welding metal E110 have cavitation resistance close to that of the stainless steels. The welds show higher cavitation resistance than their base metals because of their higher hardness and finer microstructure [15-16]. The 304L metastable austenitic stainless steel is an exception because of its high strain hardening, associated with deformation induced martensitic transformation [17-18]. Hammer-peening of the E110 weld improves cavitation resistance due to deformation hardening. It is also an indication that hammer-peening did not appreciably degrade toughness and fatigue resistance,

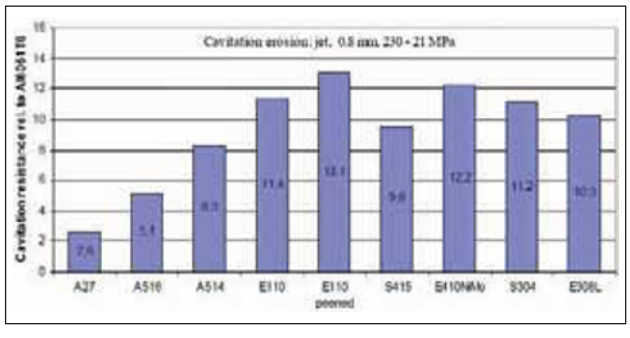

Figure 13 – Relative cavitation erosion resistance of various hydro-turbine steels and welds measured under the high pressure IREQ cavitation jet in tap water at 6 to 14 °C

as these properties are correlated with cavitation resistance [19-21].

CONCLUSION

1. Robotic welding can produce sound, defect-free, multi-pass welds, with excellent as welded tensile and toughness properties in thick plate (50 and 75 mm) of high yield strength (800 MPa), quenched and tempered steel grade A514 (S690Q).

2. Welding residual stresses measured by strain gauges and the contour method are much higher for the high strength carbon steel A514 than for the martensitic stainless steel S415, due to the low temperature martensitic transformation of the S415.

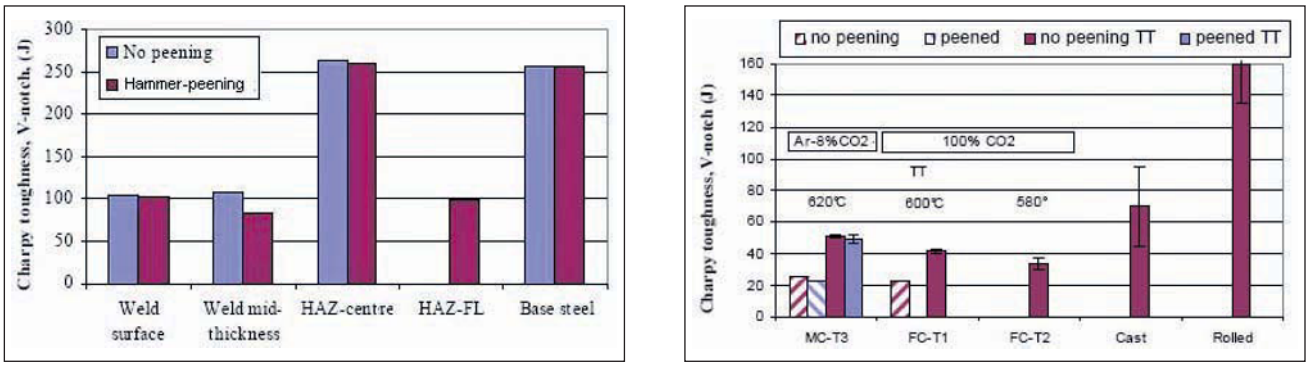

a) A514-2po, E110, -20 °C **b) E410NMo, cast CA6NM, rolledS41500, 0 °C**

Figure 12 – Charpy V-notch toughness measured on the weld and base materials for both steels

3. The highest tensile residual stress, close to the yield strength for the A514, is located at the centre of the weld deposit within the material. The stresses are lower at the surface and at the last weld bead location.

4. Hammer-peening of each weld bead has reduced transverse tensile residual stress measured on the back face of the plates by as much as 44 % in the 75 mm plate.

5. Hammer-peening of the last weld layer produces a 6 mm compression layer at the surface of the weld and eliminates any tensile stress from the plate-welded surface.

6. The E110 class weld shows high toughness without any post-weld heat treatment (around 100 Joules). Hammer-peening of the weld has not significantly deteriorated the measured Charpy V-notch energy of the weld and of the HAZ. The as-welded E410NiMo showed poor toughness with a slight improvement with post-weld heat treatment.

7. The tested ASTM A514 showed cavitation erosion resistance slightly lower than S41500 stainless steel. Both E110 and E410NiMo welds have comparable cavitation resistance, which is slightly higher than that of their base metals. Hammer-peening of the E110 weld slightly improves its cavitation resistance.

ACKNOWLEDGEMENTS

The authors wish to express their gratitude to the numerous colleagues and collaborators who conducted the experimental work: Jacques Lanteigne, René Dubois, Stéphane Godin, Carlo Baillargeon, Alexandre Lapointe, Yvan Laroche, Lyes Hacini, Sébastien Lortie and Vincent Cloutier.

REFERENCES

[1] Busque L.W.: Using robot welders to fix tunnel leak at Sainte-Marguerite 3, Hydro Review, 2005, pp. 22-26.

[2] Fihey J.-L., Simoneau R., Lanteigne J., Thibault D., Laroche Y.: Controlled hammer peening on a restrained A514 (S690Q) weldment, High Strength Steels for Hydropower Plants, Graz, Austria, Technische Universitat Graz, 2005.

[3] Debiez S., Gaillard R.: Le martelage des soudures entre passes (Hammer peening of welds between beads), CETIM informations, 1990, vol. 118, pp. 58-60.

[4] Prime M.B.: Cross-sectional mapping of residual stresses by measuring the surface contour after a cut, Journal of Engineering Materials and Technology, 2001, vol. 123, pp. 162-168.

[5] Prime M.B., Hill M.R., DeWald A.T., Sebring R.J., Dave V.R., Cola M.J.: Residual stress mapping in welds using the contour method, Trends in welding research, S.A. David, Ed., Pine Mountain, Georgia, ASM International, 2003, pp. 891-896.

[6] Prime M.B., Hughes D.J., Webster P.J.: Weld application of a new method for cross-sectional residual stress mapping, SEM Annual conference on experimental and applied mechanics, Portland, Oregon, ASM, 2001, pp. 608-611.

[7] Hacini L., Van Le N., Bocher P.: Effect of impact energy on residual stresses induced by hammer peening of 304L plates, J. Mater. Process Tech., 2008, vol. 208, no. 1-3, pp. 542-548.

[8] Simoneau R.: Vibratory, jet and hydroturbine cavitation erosion, The First ASME-JSME Fluids Engineering Conference, Portland, Oregon, USA, ASME, 1991, pp. 211-218.

[9] Simoneau R., Bourdon P.: Erosion and impact intensity of vibratory, jet and turbine cavitation, 16th IAHR Symposium on Hydraulic Machinery, Sao Paolo, Brazil, IAHR, 1992.

[10] Thibault D., Thomas M., Bocher P.: Residual stress and microstructure in welds of 13%Cr- 4%Ni martensitic stainless steel, Journal of Materials Processing Technology, 2009, vol. 209, no. 4, pp. 2195-2202.

[11] Zenitani S., Hayakawa N., Yamamoto J., Hiraoka K., Morikage Y., Kubo T., Yasuda Y., Amano K.: Development of new low transformation temperature welding consumable to prevent cold cracking in high strength steel welds, Quarterly Journal of the Japan Welding Society, 2005, vol. 23, no. 1, pp. 95-102.

[12] Mabelly Ph., Bourges Ph., Pont G.: Effect of metallurgical transformations on weld residual stresses - application to E690 steel grade, Marine Structures, 2001, vol. 14, pp. 553-567.

[13] Ohta A., Watanabe O., Matsuoka K., Maeda Y., Suzuki N., Kubo T.: Fatigue strength improvement of box welds by low transformation temperature welding wire and PWHT, Doc. IIW-1480-89 (ex-doc XIII-1758-99), Welding in the World, 2000, vol. 44, no. 3, pp. 52-56.

[14] Martinez F., Liu S., Edwards G.: The development of a compressive residual stress around a structural steel weld by means of phase transformations, Joining of advanced and specialty materials, Columbus, Ohio, ASM International, 2004.

[15] Thiruvengadam A.: Handbook of Cavitation Erosion, National Technical Information Service, Springfield, VA, USA, AD-787 073, 1974.

[16] Simoneau R., Lambert P., Simoneau M., Dickson J.I., L'espérance G.: Cavitation erosion and deformation mechanisms of Ni and Co austenitic stainless steels, Seven International Conference on Erosion by Liquid and Solid Impact, ELSI VII, Cambridge, UK, University of Cambridge, 1987.

[17] Woodford D.A.: Cavitation-erosion-induced phase transformation in alloys, Metallurgical Transactions, 1972, vol. 3, no. May, pp. 1137-1145.

[18] Heathcock C.J., Protheroe B.E.: Cavitation Erosion of Stainless steel, Wear, 1982, vol. 81, pp. 311-327.

[19] Hammitt F.G.: Cavitation and multiphase flow phenomena, New York, USA, McGraw-Hill, 1980.

[20] Syamala Rao B.C., Veerabhadra Rao P., Lashmana Rao N.S.: Evaluation of erosion resistance of metallic materials and the role of material properties in correlations, Journal of testing and evaluation, 1979, vol. 7, no. 3, pp. 133-146.

[21] Richman R.H., McNaughton W.P.: Correlation of cavitation erosion behavior with mechanical properties of metals, Wear, 1990, vol. 140, pp. 63-82.